The Search for an Atmospheric Signature of the Transiting Exoplanet HD 149026b[1]

Nassim Bozorgnia,[2] Jonathan J. Fortney,[3,4,5] Chris McCarthy,[2] Debra A. Fischer,[2] and Geoffrey W. Marcy[2,6]

ABSTRACT. HD 149026b is a short-period, Saturn-mass planet that transits a metal-rich star. The planet's radius, determined by photometry, is remarkably small compared to other known transiting planets, with a heavy-element core that apparently comprises ~70% of the total planet mass. Time-series spectra were obtained at Keck before and during transit in order to model the Rossiter-McLaughlin effect. Here we make use of these observations to carry out a differential comparison of spectra obtained in and out of transit to search for signatures of neutral atomic lithium and potassium from the planet atmosphere. No signal was detected at the 2% level; we therefore place upper limits on the column density of these atoms.

Online material: color figures

1. INTRODUCTION

Extrasolar planets that transit their host stars offer a unique opportunity to search for constituents in the planet atmosphere. As stellar flux passes through the planet atmosphere, additional absorption features will be imprinted on the (otherwise pure) stellar spectrum (Seager & Sasselov 2000; Brown 2001; Hubbard et al. 2001). This offers a possibility for detection of atmospheric transmission features when working differentially with in-transit and out-of-transit spectra. We have used this fact to search for additional absorption in alkali lines from the atmosphere of HD 149026b during transit.

Transiting planets that reside close to their host stars are strongly irradiated and have atmospheres with temperatures (but not gravities) similar to those of late-type L dwarfs. In the cool atmosphere of substellar objects such as brown dwarfs and giant exoplanets, the more refractory metals condense and rain out of the atmosphere, leaving the less refractory alkali metals in atomic form (Burrows & Sharp 1999; Lodders 1999). Thus, the strongest absorption features are expected for alkali metals such as sodium and potassium (Seager & Sasselov 2000; Sudarsky et al. 2000).

Since the discovery of HD 209458b (Charbonneau et al. 2000; Henry et al. 2000), this star has been the subject of many ground- and space-based studies. HD 209458 is a bright star with $V = 7.65$, permitting spectroscopy with high resolution and a high signal-to-noise ratio (S/N). The transiting planet has an anomalously large radius of $1.3R_J$, making it an excellent candidate to search for atmospheric signatures. In contrast, searching for atmospheric features in other transiting exoplanets may be more difficult, because the planet-to-star radius is generally smaller and the host stars have a lower intrinsic brightness. However, if other exoplanets have tenuous but extended atmospheres, then it may be possible to identify atmospheric features from the planet.

The most successful searches for exoplanet atmospheres have been carried out from space, where telluric contamination is avoided and higher S/N has enabled more sensitive searches. Based on observations with the *Hubble Space Telescope* (*HST*), Charbonneau et al. (2002) detected absorption from the sodium resonance doublet at 5893 Å in the dense lower atmosphere of HD 209458b, and Vidal-Madjar et al. (2003) detected an escaping, trailing extended exosphere of hydrogen. In contrast, it is more challenging to search for exoplanet atmospheres with ground-based telescopes. Bundy & Marcy (2000) carried out a differential analysis of spectra for HD 209458 obtained in and out of transit at the Lick and Keck Observatories. They also studied the spectra of 51 Pegasi, which is not a transiting planet. Because of contamination from H_2O and O_2 features, they were only able to place weak upper limits on Na I and K I line depth variations. Deming et al. (2005) searched for carbon monoxide absorption features in the transmission spectrum of HD 209458b at ~2.3 μm using NIRSPEC on the Keck II Telescope. Their analysis required 1077 high-resolution spectra in order to achieve comparable sensitivity to the *HST* sodium observations. No changes in the CO features in and out of transit were measured, implying the presence of high clouds in the planet's atmosphere.

[2] Department of Physics and Astronomy, San Francisco State University, 1600 Holloway Avenue, San Francisco, CA 94132; fischer@stars.sfsu.edu.

[3] Space Science and Astrobiology Division, NASA Ames Research Center, MS 245-3, Moffett Field, CA 94035; jfortney@arc.nasa.gov.

[4] *Spitzer* Fellow.

[5] SETI Institute, 515 North Whisman Road, Mountain View, CA 94043.

[6] Department of Astronomy, University of California, Berkeley, 601 Campbell Hall, Berkeley, CA 94720.

2. HD 149026: A STAR WITH A TRANSITING PLANET

HD 149026 is a metal-rich G0 IV subgiant with $V = 8.15$ and an absolute visual magnitude $M_V = 3.66$. The planet's mass is similar to that of Saturn in our solar system, with a radius of $0.725R_J$ (Sato et al. 2005), determined from the observed photometric transit depth. Interior models discussed by Sato et al. (2005) imply a planet core of about 70 $M_\oplus$. HD 149026b orbits with a semimajor axis of only $a = 0.045$ AU, and Sato et al. (2005) report an effective temperature of 1540 K in the planet atmosphere.

2.1. Expected Atmospheric Features

The equilibrium temperature of an exoplanet atmosphere at the substellar point is a function of the effective stellar temperature T_*, the stellar radius R_*, and the planet-star separation a. These factors are modulated by the planet Bond albedo A_B, and by a geometrical factor f. If a thermal gradient is established from heating on the tidally locked day side of the planet, then a wind will circulate energy to the night side of the planet. Depending on the efficiency of this process, f is 1 for isotropic emission from both sides of the planet and scales to 2 for emission from the day side only. The equilibrium temperature is thus

$$T_{eq} = T_*(R_*/2a)^{1/2}[f(1 - A_B)]^{1/4}. \qquad (1)$$

Adopting T_* and R_* from Sato et al. (2005), and assuming isotropic emission and a Bond albedo $A_B = 0.3$, we calculate $T_{eq} = 1593$ K.

Fortney et al. (2006) define the planet effective temperature as

$$T_{eff}^4 = T_{eq}^4 + T_{int}^4, \qquad (2)$$

where T_{eq} is the equilibrium temperature of the planet in the presence of stellar radiation, and T_{int} is the effective intrinsic temperature of the planet in isolation. These authors note that for strongly irradiated planets, the intrinsic isolation temperature is negligible. They consider atmospheric models for HD 149026b with a range of metallicities: [M/H] = 0, 0.5, 1.0. For a cloud-free model with [M/H] = 0.5 and assuming isotropic radiation, Fortney et al. (2006) derive an effective temperature of 1734 K for the planet atmosphere, implying $A_B <$ 0.1. If radiation is not isotropic, but radiates from the day side only (2π sr), this same atmospheric model yields $T_{eff} =$ 2148 K, and TiO and VO features appear at low pressures (Fortney et al. 2006).

The temperature of HD 149026b is therefore likely to be similar to the temperature of L/T dwarfs (Kirkpatrick 2005). The brown dwarf spectral sequence is a temperature sequence over part of the range, except from mid/late L to mid T, where the behavior of clouds becomes a dominant effect (Kirkpatrick

2005). The effective temperature estimates for HD 149026b, ranging from 1540 to 2148 K, correspond to the brown dwarf spectral type range from early L to mid T.

Based on the effective temperature range of the planet, observable spectral features in the atmosphere can be predicted. The spectra of L dwarfs, T dwarfs, and irradiated giant planets have dominant absorption lines from neutral alkali metals such as Na I, K I, Rb I, Cs I, and Li I. Early L-type dwarfs have prominent molecular lines, TiO and VO bands, and hydride bands FeH, CaH, and CrH in their atmospheres. By mid to late L types, the hydrides and the ground-state neutral lines of Na I and K I have grown in strength and are the dominant absorbers, while the TiO and VO have weakened. Another important feature in the spectra of late L-type and mid T-type brown dwarfs is H_2O; the neutral alkali lines are still strong, and the hydrides are less prominent. In late T-type brown dwarfs, the two major lines of Na I and K I have grown very wide (Kirkpatrick 2005). Because the rainout of condensates clears the atmosphere of most of its metals, the less refractory neutral alkali metals become important in the atmospheres of strongly irradiated, close-in (~0.05 AU) exoplanets with T_{eff} from 800 to 2000 K (Burrows & Volobuyev 2003; Sudarsky et al. 2003). Sodium and potassium can be particularly important in both brown dwarfs and the hotter ($\geq$1400 K) of the giant exoplanet classes. Other alkali metals such as lithium should also be present in giant exoplanets, but with lower abundances (Sudarsky et al. 2003). Fortney et al. (2006) find that model atmospheres of HD 149026b with [M/H] = 0.5 should show strong absorption by Na and K in the optical spectra. As the *majority* of the planet's mass must be made up of metals, the metallicity of the atmosphere of HD 149026b could be quite high.

2.2. Observations

A total of 30 spectra of HD 149026 were obtained at the Keck I Telescope, using the HIRES echelle spectrometer (Vogt et al. 1994). Eighteen of these spectra were obtained while the planet was transiting the host star. The spectra have a resolution of $R \sim 55,000$ and span a wavelength range of 3500–8000 Å, with a typical S/N of 250. All of these observations were obtained in order to derive velocity information about the star and to model the Rossiter-McLaughlin effect (Wolf et al. 2006). The Rossiter-McLaughlin effect is an apparent deviation in the radial velocity from a Keplerian orbit. This occurs when an extrasolar planet transits across the face of its host star, first obscuring the approaching limb of the rotating star and then the receding limb of the star. The resulting line profile variations at the blue and red edges of the spectral lines are spuriously interpreted as a Doppler shift in our analysis.

In order to carry out Doppler analysis, an iodine cell is positioned in front of the spectrometer slit to imprint narrow reference iodine lines. These iodine lines span the wavelength range 4800–6200 Å and have a depth of about 20%. The iodine
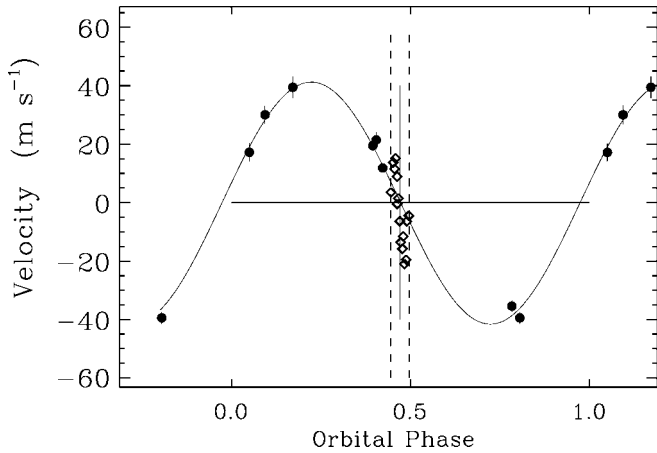
FIG. 1.—Updated phased radial velocities for HD 149026. The velocities measured at Keck during transit are shown as open diamonds in the plot. These measurements exhibit the Rossiter-McLaughlin effect and were removed when fitting a Keplerian model. [*See the electronic edition of PASP for a color version of this figure.*]

FIG. 2.—Template nontransit spectrum for the K line overplotted on a transit spectrum. The difference of the two (offset from zero) and the 10.4 km s^{-1} wavelength bin (*dashed lines*) are also shown.

lines are used to measure wavelength shifts (velocities) and to derive the instrumental point-spread function; however, they interfere with our ability to measure small changes in line absorption strengths. Unfortunately, the Na I doublet is contaminated by the presence of iodine and could not be included in our analysis.

Redward of 6000 Å, telluric lines begin to appear in the stellar spectrum. Differences in barycentric velocities at the times of observations create significant shifts in the stellar spectrum relative to the telluric features. Telluric lines that shift in and out of the spectral lines in our analysis are problematic because they will introduce a spurious signal. To avoid this problem, we cross-correlated a telluric spectrum with each stellar spectrum and masked the regions of the spectra containing telluric lines. For those cases in which the telluric lines fall on a stellar line, we masked out the entire spectral line in order to avoid introducing large errors. Doppler shifts arising from dynamical orbital motion correspond to subpixel shifts and can be ignored.

3. ANALYSIS

Our goal was to search for constituents of the illuminated planet atmosphere during transit. In order to carry out the strongest possible analysis, we worked differentially, comparing spectra obtained during transit with those obtained out of transit. As a first step, we identified the in-transit and out-of-transit spectra by phase-folding the radial velocity (RV) data with a period of $P = 2.875965^{+0.000085}_{-0.000135}$ days. This value was calculated by taking the mean of the values provided by Charbonneau et al. (2006) and Wolf et al. (2006), which agree with each other within the stated uncertainties. The time at the center of transit,
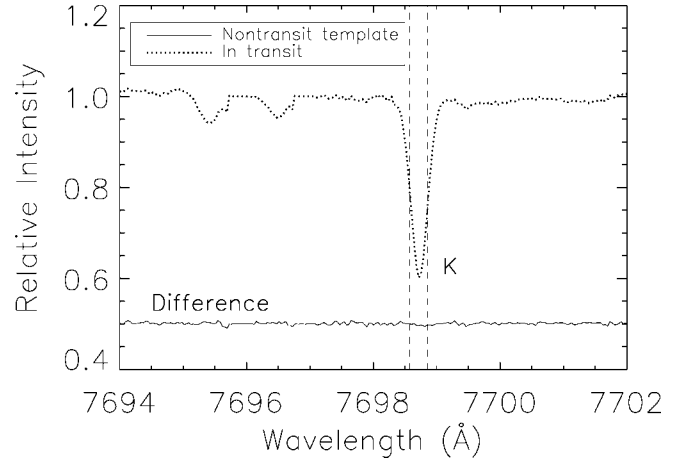
$T_c =$ HJD $2,453,527.87455^{+0.00085}_{-0.00091}$, was adopted from Charbonneau et al. (2006).

Figure 1 represents an update to the phased RV data for HD 149026 presented in Sato et al. (2005). The Keplerian fit is overplotted on the RV data. Fifteen RV measurements made at Keck during transit are shown as open diamonds in the plot. These points were removed when fitting the Keplerian model, because they exhibit the Rossiter-McLaughlin effect and deviate from Keplerian velocities. We froze the period at $P = 2.87596$ days to make this fit, and the rms RV scatter to the fit is 3.07 m s^{-1}, consistent with our velocity precision. The dashed lines in the plot show the 215 minute transit window.

We constructed a high-S/N, continuum-normalized template for HD 149026 by averaging all 12 nontransit spectra. Each individual spectrum (both in and out of transit) was normalized and cross-correlated with the template spectrum. As a first step, we divided each spectrum by the template and searched the full wavelength range of 6500–8000 Å by eye for any residuals relative to the template spectrum. We examined nine spectral orders this way and found no significant changes in the spectrum greater than a few percent. Because of contamination from telluric and iodine lines, we were not able to make use of other spectral orders.

We then carried out a more robust analysis by searching individual lines, such as potassium and lithium, in detail. We considered a wavelength bin centered on the K line at 7698 Å. The template spectrum is overplotted on an in-transit spectrum in Figure 2. The difference of the two spectra (offset from zero) and the line-core bin for the K line are also shown in the same figure. We calculated the percentage deviation at each pixel by taking the difference between each spectrum and the template spectrum and dividing by the template spectrum. In order to average over photon noise, we binned the percentage difference in wavelength, choosing bins with widths that were comparable
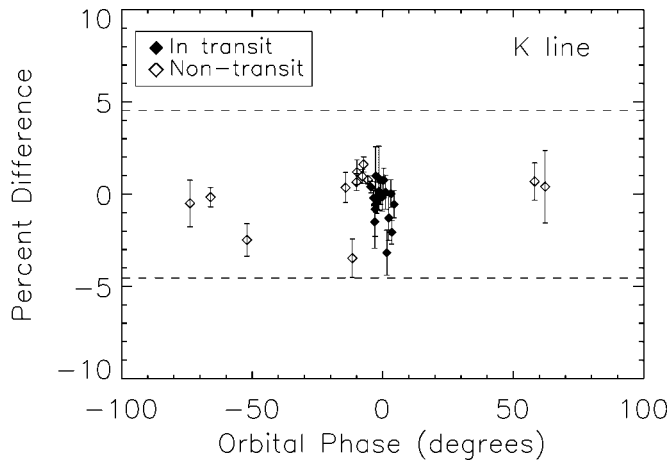
FIG. 3.—Deviations of the K line. The percentage deviation is averaged over the 10.4 km s^{-1} bin. This percentage deviation was calculated by taking the difference between each spectrum and the template nontransit spectrum (which was constructed by averaging 12 nontransit spectra) and dividing by the value of the template spectrum. The dashed lines indicate the 3 σ detection limits, where σ is the rms scatter in the out-of-transit spectra. [*See the electronic edition of PASP for a color version of this figure.*]

to the sizes of the absorption-line cores (8 pixels, or 10.4 km s^{-1}). The percentage deviations are plotted with respect to orbital phase in Figure 3.

The individual spectra have S/Ns better than 250, so we expect the photon noise to be about 0.4% in the continuum, but larger in cores of the spectral lines. In addition to photon noise, there are systematic errors that arise from imperfect continuum normalization, from the uncertainties in vertically registering the individual spectra against the template, from spectrum-to-spectrum variations in weak telluric lines, and perhaps from trace iodine features.

To assess our uncertainties, we computed the standard deviation of the percentage differences for 12 *out-of-transit* spectra in the wavelength bins of interest. Since the out-of-transit spectra should not be contaminated by the planet atmospheres, this represents the typical uncertainties, including Poisson errors and systematic errors. The dashed lines in Figure 3 show the limits where the variations would have exceeded 3 times the intrinsic fluctuations measured in the out-of-transit spectra.

A Kolmogorov-Smirnov (K-S) test was applied to the in-transit and out-of-transit residuals and suggests that both sets of spectra were drawn from the same parent population. The probability that the two samples were drawn from different populations is only 0.36%, implying that there is no evidence for an excess of potassium in the irradiated planet atmosphere.

The same analysis was applied to the Li I resonance doublet at 6707.82 Å. Figure 4 shows a comparison of the template and an in-transit spectrum; the 10.4 km s^{-1} bin used for the lithium line is also plotted in the same figure. The percentage deviations for Li are shown in Figure 5, and the dashed lines
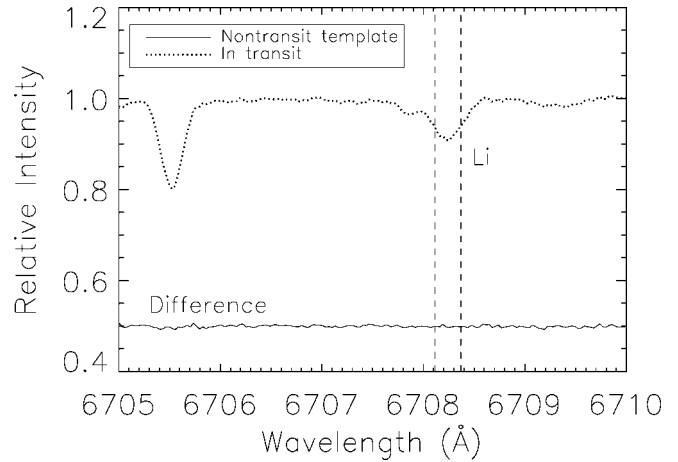

FIG. 4.—Template nontransit spectrum for the Li line overplotted on a transit spectrum. The difference of the two (offset from zero) and the 10.4 km s^{-1} wavelength bin (*dashed lines*) are also shown.

show the limit of 3 times the intrinsic fluctuations measured in the out-of-transit spectra. Again, the K-S test shows that the in-transit spectra are statistically indistinguishable from the out-of-transit spectra; no excess lithium absorption is seen during transit.

We also scrutinized observations taken near ingress and egress times, for evidence of a leading or trailing atmosphere that could enhance absorption when the planet is not actually transiting. To investigate this possibility, we modified our original analysis of the potassium and lithium lines. In this analysis, we constructed a template spectrum from only five out-of-transit spectra that were clearly not near the ingress and egress points. We then repeated the analysis described above for the K and Li lines. Figure 6 shows the percentage deviations for
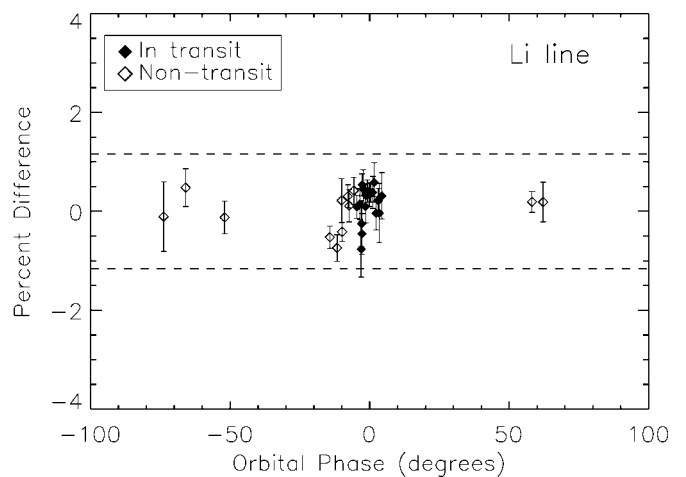

FIG. 5.—Same as Fig. 3, but for the Li line. [*See the electronic edition of PASP for a color version of this figure.*]
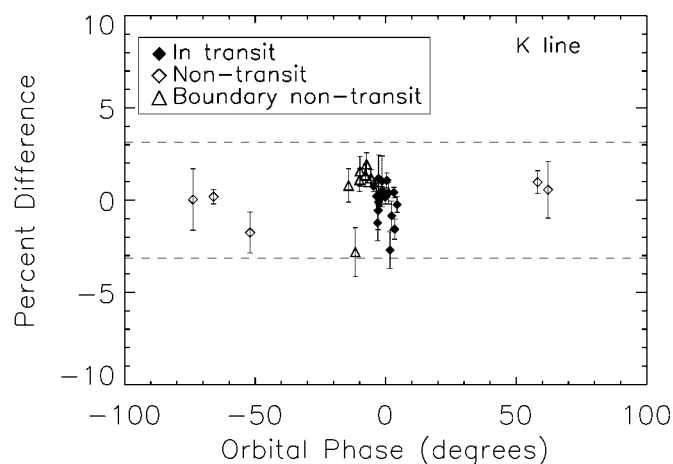
FIG. 6.—Deviations of the K line. These deviations were computed using a template spectrum that was constructed from five nontransit spectra. The triangles show the boundary nontransit observations that were close to the ingress and were not used in the template nontransit spectrum. [*See the electronic edition of PASP for a color version of this figure.*]

FIG. 7.—Same as Fig. 6, but for the Li line. [*See the electronic edition of PASP for a color version of this figure.*]

individual observations of the K line relative to the new template and plotted against orbital phase. Figure 7 shows the percentage deviations for the Li I line as a function of orbital phase. The dashed horizontal lines again show boundaries that represent 3 times the rms scatter in the five nontransiting spectra. The nontransit observations near ingress or egress are shown as boundary nontransit points (*open triangles*) in the plot. Again, the K-S test shows that the line depths do not vary significantly, whether the observation was obtained in transit, near ingress or egress, or out of transit. Therefore, we see no line enhancement that suggests a leading or trailing exosphere with a large optical depth.

4. DETECTABILITY SIMULATIONS

To determine the increase in optical depth in the planet atmosphere that would be needed to produce a detectable signal, we generated synthetic spectra with injected planetary signals of different strengths. We scaled the K and Li lines in 1% steps for each of our *in-transit* spectra. For each of these pseudo–optical depth scaling factors, we applied the two-sided K-S test to find the probability that the simulated transit data were drawn from the same distribution as our out-of-transit template. For our analysis, we used the template constructed from five observations that were not close to ingress or egress. The pseudo–optical depth scaling factors for the K line and the resulting K-S statistic, as well as the detection probabilities, are listed in Table 1. Small values of the K-S statistic show that the cumulative distribution function of our scaled-up in-transit spectra is significantly different from the out-of-transit template and therefore yields a high probability of detection. Alternatively, the detection probability is 1 minus the K-S statistic. A
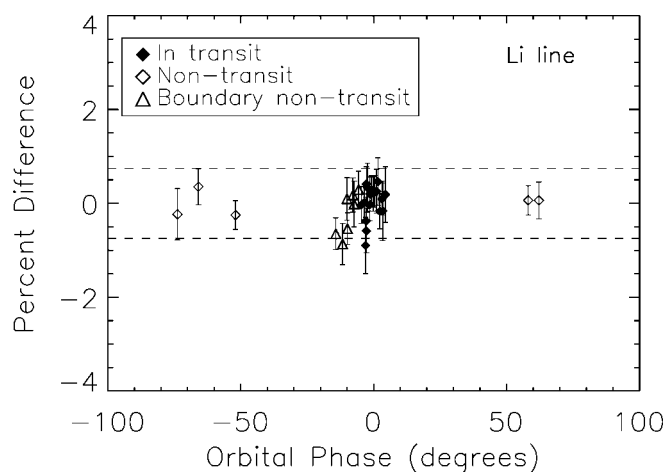
signal with a 1.03 pseudo–optical depth scaling factor would have been detected at the 95.16% confidence level.

Figure 8 shows a comparison of in-transit data with a 1.02 pseudo–optical depth scaling for the K line. This synthetic data set represents a transit by a planet that imprints a spectral signature that is 2% stronger than the signal already present in the stellar spectrum. The top panel shows an overplot of the template and synthetic spectra. We subtracted the template from the synthetic spectrum and offset the differences from zero for visibility on the same scale. The bottom plot in Figure 8 shows the percentage deviations for the out-of-transit and synthetically enhanced in-transit data relative to the template. The K-S test compares these two populations (out-of-transit data and synthetic in-transit data) to calculate the detection probability listed in Table 1.

Figure 9 shows the synthetic signal corresponding to a 1.05 pseudo–optical depth scaling factor for the K line. As with Figure 8, the simulated change of 5% in the transit spectra is overplotted on the template in the top plot. Figure 9 (*bottom*) shows the percentage difference in the 10.4 km s^{-1} bin. A K-S test finds a detection probability of 98.8% for this case. Finally, Figure 10 shows the fake injected signal for a pseudo–

TABLE 1
K-S TEST FOR POTASSIUM

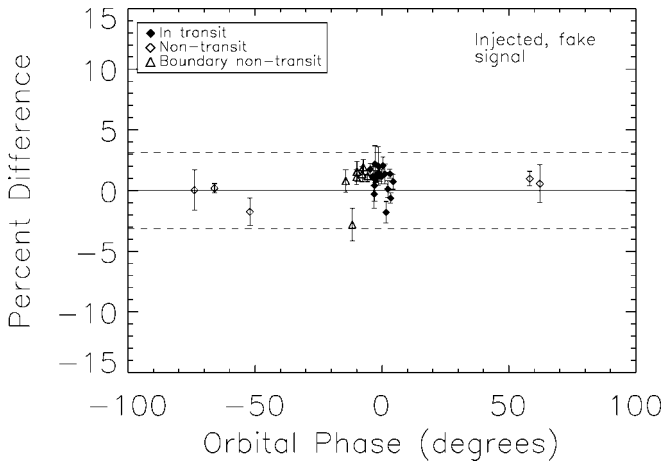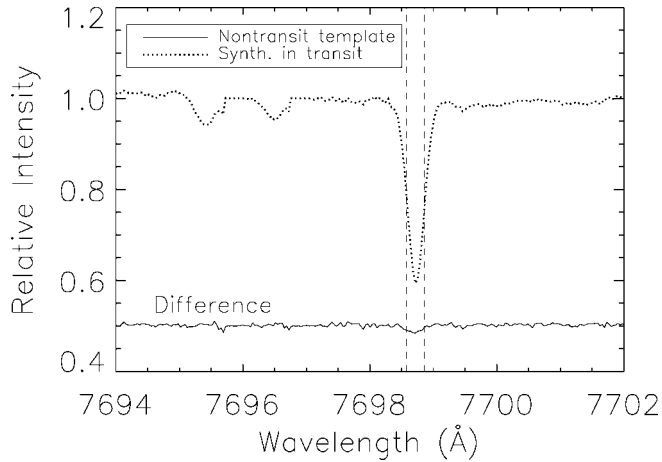| Pseudo–Optical Depth Scaling Factor	K-S Significance Level	Detection Confidence Level (%)
1.00	0.9964	0.36
1.01	0.4131	58.69
1.02	0.1592	84.08
1.03	0.0484	95.16
1.04	0.0245	97.55
1.05	0.0117	98.83
1.08	0.0053	99.47

FIG. 8.—Synthetic data with a 2% signal introduced at 7698 Å. *Top*: Synthetic transit spectrum overplotted on the template nontransit spectrum. The difference (offset from zero) is also plotted. *Bottom*: Percentage deviations for such a signal. There is an 84% confidence level to detect such a signal. [*See the electronic edition of PASP for a color version of this figure.*]
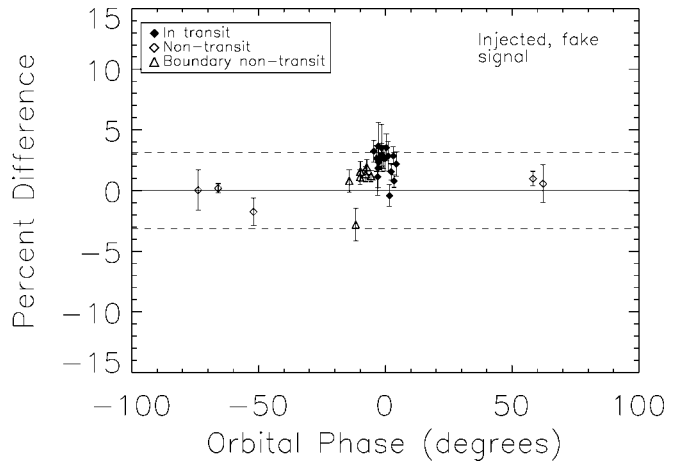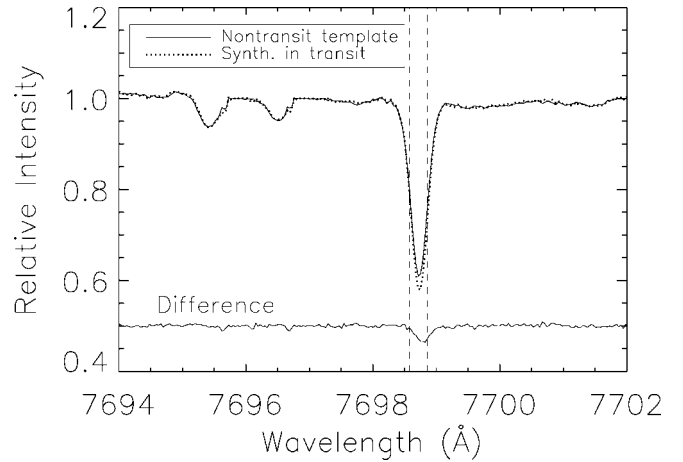
FIG. 9.—Synthetic data with a 5% signal introduced at 7698 Å. *Top*: Synthetic transit spectrum overplotted on the template nontransit spectrum. The difference (offset from zero) is also plotted. *Bottom*: Percentage deviations for such a signal. There is a 98.8% confidence level to detect such a signal. [*See the electronic edition of PASP for a color version of this figure.*]

optical depth factor of 1.08 at the place of the K line. Clearly, an enhancement in line depth of 8% could even be discovered by simple inspection.

We carried out a similar scaling for the Li line at the 10.4 km s^{-1} bin at 6707.8 Å and simulated a line with deeper strength. Table 2 shows different values of the pseudo–optical depth scaling factor, their corresponding K-S significance level, and the confidence level for detecting the signal. A pseudo–optical depth scaling factor of 1.02 results in a 84% confidence level for detecting lithium, and for a scaling factor of 1.08, the confidence level for detecting the signal is 98.8%.

5. DISCUSSION

The detection of absorption features in the lower atmosphere of a transiting giant planet requires outstanding precision. Char-

bonneau et al. (2002), who detected neutral atomic sodium, and Deming et al. (2005), who placed upper limits on CO absorption, obtained a 100 times better precision for HD 209458 than we have in our study. They were looking for 0.02% effects. These studies made use of the *Hubble Space Telescope* and over 1000 ground-based spectra, respectively. However, the detection of species in an extended exosphere need not necessarily require this same precision, because the atmosphere's cross-sectional area is significantly larger (Vidal-Madjar et al. 2003).

If one thinks of our 2% precision as the smallest cross-sectional atmospheric area that we could observe, this corresponds to $2.1R_J$ on top of the opaque-at-all-wavelengths $0.725R_J$ planet. This large distance makes it immediately clear that we would only be sensitive to species in a large extended exosphere, such as that observed by Vidal-Madjar et al. (2003).
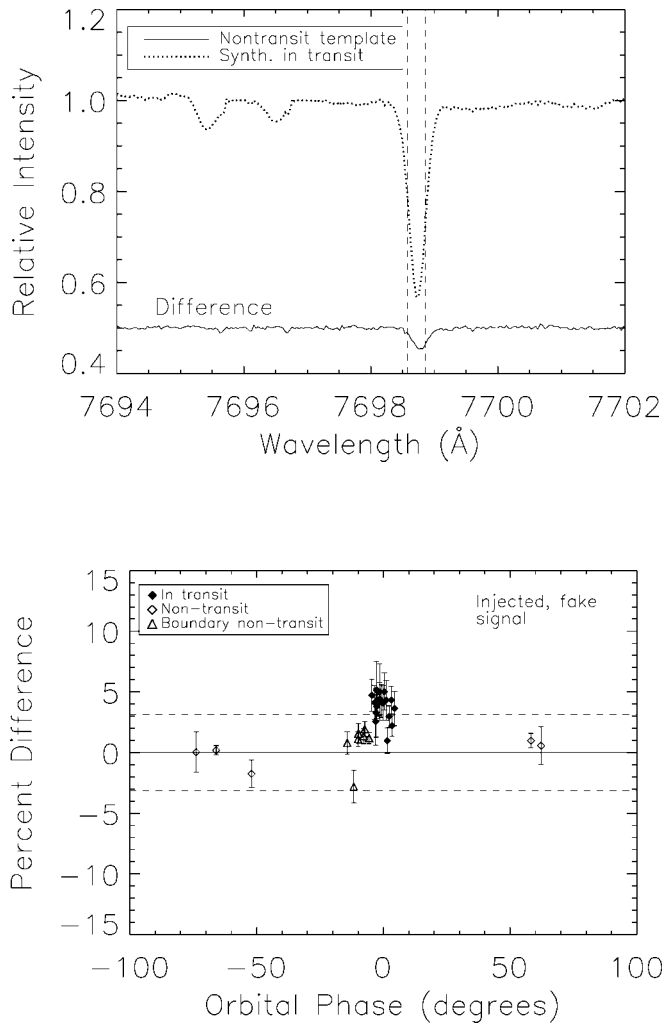
Pseudo–Optical Depth Scaling Factor	K-S Significance Level	Detection Confidence Level (%)
1.00	0.6007	39.93
1.01	0.4131	58.69
1.02	0.1592	84.08
1.03	0.0484	95.16
1.06	0.0245	97.55
1.08	0.0117	98.83

have an equal abundance. This curve has only weak pressure dependence. At the lowest pressure considered, 1 mbar, K I and K II are equal in abundance at a temperature of 1900 K. Our exospheric temperatures are likely 5–10 times hotter, meaning K II is strongly preferred. Photodissociation is also likely important and will further reduce the abundances of Li I and K I. Fortney et al. (2003) examined ionization of Na in the atmosphere of HD 209458b and found that photoionization of this species on the planet's limb could proceed to pressures as high as ~1 mbar. The atoms Li and K have even lower ionization potentials. Due to the high temperatures and strong photoionizing flux, it appears unlikely that neutral atomic Li and K will be found in significant abundance in the extended atmosphere of HD 149026b. This is consistent with the observations of Charbonneau et al. (2002), who observed Na I in the lower atmosphere, but not the exosphere, of HD 209458b.

R. S. Freedman has kindly provided us with absorption cross sections as a function of wavelength for K and Li across our observation bands. These are $\sim 4 \times 10^{-13}$ cm^2 for Li and $\sim 1 \times 10^{-13}$ cm^2 for K. Since we find that the exosphere has an optical depth $\lesssim 1$ at $2.1 R_J$, this corresponds to column densities for these atoms in their neutral atomic ground states, of $\lesssim 2 \times 10^{12}$ cm^{-2} for Li and $\lesssim 9 \times 10^{12}$ cm^{-2} for K at this radius.

A more sensitive search from space-based telescopes could result in a detection of the planetary atmosphere. Ionized alkali species would have noble gas electron configurations and would not have prominent absorption features, even for space-based observations. We advocate a search for H Lyα from space to give a first estimate of the extent of an exosphere in HD 149026b. At the same time, since there is a clear link between heavy-element mass and atmospheric metallicity in the giant planets in our own solar system, the atmosphere and exosphere of HD 149026b could be richer in metals than HD 209458b. The next elements to search for would probably be C, N, and O species.

Fig. 10.—Synthetic data with an 8% signal introduced at 7698 Å. *Top*: Difference (offset from zero) of the synthetic transit spectrum and the template nontransit spectrum. *Bottom*: Percentage deviations for such a signal. Such a signal would clearly be detected. [*See the electronic edition of PASP for a color version of this figure.*]

Therefore, only if K and Li had a large enough column abundance to remain optically thick past $2.1 R_J$ would these atoms have been detected.

Furthermore, these species must remain neutral and atomic, such that they would absorb stellar flux at our specified wavelengths. While these species are likely neutral in the lower atmosphere around $P \gtrsim 1$ mbar, where Charbonneau et al. (2002) detected Na in HD 209458b, all exospheric models for highly irradiated giant planets predict temperatures on the order of 10^4 K (Lammer et al. 2003; Yelle 2004; Tian et al. 2005). Based on calculations by Yelle (2004) for an HD 2094358b–like planet at 0.04 AU, $2.1 R_J$ likely corresponds to $P \sim 10^{-10}$ bars and $T \sim 2 \times 10^4$ K. This high temperature makes it likely that Li and K will be ionized. Examining K specifically, Lodders & Fegley (2006) review the chemistry of alkalis in substellar atmospheres and plot a curve in which K I and K II

REFERENCES

Brown, T. M. 2001, ApJ, 553, 1006

Bundy, K. A., & Marcy, G. W. 2000, PASP, 112, 1421

Burrows, A., & Sharp, C. M. 1999, ApJ, 512, 843

Burrows, A., & Volobuyev, M. 2003, ApJ, 583, 985

Charbonneau, D., Brown, T., Latham, D., & Mayor, M. 2000, ApJ, 529, L45

Charbonneau, D., Brown, T. M., Noyes, R. W., & Gilliland, R. L. 2002, ApJ, 568, 377

Charbonneau, D., Winn, J. N., Latham, D. W., Bakos, G., Falco, E. E., Holman, M. J., Noyes, R. W., & Csák, B. 2006, ApJ, 636, 445

Deming, D., Brown, T. M., Charbonneau, D., Harrington, J., & Richardson, L. J. 2005, ApJ, 622, 1149

Fortney, J. J., Saumon, D., Marley, M. S., Lodders, K., & Freedman, R. S. 2006, ApJ, 642, 495

Fortney, J. J., Sudarsky, D., Hubeny, I., Cooper, C. S., Hubbard, W. B., Burrows, A., & Lunine, J. I. 2003, ApJ, 589, 615

Henry, G. W., Marcy, G. W., Butler, R. P., & Vogt, S. S. 2000, ApJ, 529, L41

Hubbard, W. B., Fortney, J. J., Lunine, J. I., Burrows, A., Sudarsky, D., & Pinto, P. 2001, ApJ, 560, 413

Kirkpatrick, J. D. 2005, ARA&A, 43, 195

Lammer, H., Selsis, F., Ribas, I., Guinan, E. F., Bauer, S. J., & Weiss, W. W. 2003, ApJ, 598, L121

Lodders, K. 1999, ApJ, 519, 793

Lodders, K., & Fegley, B. 2006, in Astrophysics Update 2, ed. J. W. Mason (Berlin: Springer), in press (astro-ph/0601381)

Sato, B., et al. 2005, ApJ, 633, 465

Seager, S., & Sasselov, D. D. 2000, ApJ, 537, 916

Sudarsky, D., Burrows, A., & Hubeny, I. 2003, ApJ, 588, 1121

Sudarsky, D., Burrows, A., & Pinto, P. 2000, ApJ, 538, 885

Tian, F., Toon, O. B., Pavlov, A. A., & De Sterck, H. 2005, ApJ, 621, 1049

Vidal-Madjar, A., Lecavelier des Etangs, A., Désert, J.-M., Ballester, G. E., Ferlet, R., Hébrard, G., & Mayor, M. 2003, Nature, 422, 143

Vogt, S. S., et al. 1994, Proc. SPIE, 2198, 362

Wolf, A., et al. 2006, ApJ, in press

Yelle, R. V. 2004, Icarus, 170, 167